Design of a variable-included-angle Monk–Gillieson monochromator with varied-line-spacing gratings

Kenta Amemiya and Toshiaki Ohta*

Department of Chemistry, Graduate School of Science, The University of Tokyo, 7-3-1 Hongo, Bunkyo-ku, Tokyo 113-0033, Japan. E-mail: ohta@chem.s.u-tokyo.ac.jp

A novel design concept is presented for a variable-included-angle Monk–Gillieson mounting monochromator with a varied-line-spacing (VLS) plane grating, in which the grating is illuminated by converging X-rays. The energy resolution for a beamline with a typical undulator source is estimated by means of the ray-tracing method. It is shown that the source-size or slope-error limited resolution is achieved in a wide energy range by properly changing the included angle. Moreover, relatively high resolution is maintained even if one scans the photon energy with a fixed included angle, which is a great advantage over the previous VLS grating monochromator with diverging illumination on the grating. A design example for a bending-magnet beamline is also presented, indicating that the new design concept is valid even for high-emittance sources.

Keywords: soft X-ray monochromators; Monk–Gillieson mountings; varied-line-spacing gratings; variable included angle.

1. Introduction

Among various kinds of grazing-incidence soft X-ray monochromators, the Monk–Gillieson mounting monochromator with a varied-line-spacing (VLS) grating (Hettrick, 1988; Hettrick *et al.*, 1988) is one of the most successfully developed optics of the last few decades, since high energy resolution is achieved by simply rotating the grating. This is because the Monk–Gillieson mounting, in which a plane grating is illuminated by X-rays converged by a pre-focusing mirror (Monk, 1928; Gillieson, 1949), gives an almost perpendicular focal plane with respect to the X-ray beam at the exit slit, especially if it is combined with a VLS grating. However, although the scanning mechanism itself is quite simple, one has to exchange gratings or pre-focusing mirrors in order to cover a wide energy range with high resolution and high photon flux. This is intrinsically inevitable in the case of fixed-included-angle monochromators. Moreover, it is difficult to suppress the higher spectroscopic orders over the whole energy range.

On the other hand, variable-included-angle monochromators with conventional (Petersen, 1982) and VLS (Itou *et al.*, 1989) gratings have been developed, which cover a wide energy range without exchanging any optical elements. They require a precise included-angle scan, however, in order to achieve high resolution, because diverging X-rays illuminate the grating in both cases, so that the focusing condition for the diffracted X-rays is quite severe. Therefore, although the higher-order suppression mode is available by properly changing the included angle, it often causes a serious deterioration of the energy resolution. Moreover, a post-focusing mirror is necessary downstream of the grating in the case of a conventional grating (Petersen, 1982).

Recently, a variable-included-angle monochromator with collimated illumination on the grating was developed, in which X-rays are collimated by a pre-mirror, reflected by a plane mirror which determines the included angle, diffracted by a plane grating, and focused by a post-mirror (Follath & Senf, 1997). Deterioration of the energy resolution is prevented, in principle, for any scan mode. However, although collimation and focusing are satisfactorily achieved with sagittal cylindrical mirrors in the case of a low-emittance undulator source, aberrations arising from these mirrors are not negligible for high-emittance sources, such as a bending magnet. Moreover, the slope error of the post-mirror affects the energy resolution more seriously than the pre-mirror.

A possibility for applying the variable-included-angle mechanism to the Monk–Gillieson mounting monochromator with a VLS grating has been proposed in order to obtain high energy resolution over a wide energy range (Koike & Namioka, 1995; Koike, 1996). Since no focusing mirror is necessary downstream of the grating, the beamline optics are rather simple and the slope error effect is relatively small. In spite of its fascinating potential, however, the design method and performance of such a monochromator has not been well discussed to date. Although some design examples were given in previous work (Koike & Namioka, 1995; Koike, 1996), their design was based on the merit function estimated from the ray-traced spots. Accordingly, no light-path function including both the pre-focusing mirror and the VLS grating has been derived, which is essential to establish a comprehensive design process. Moreover, they considered only the ideal case, where the included angle is properly altered simultaneously with the grating rotation. From the practical viewpoint, however, it is also important to investigate various combinations of the included angle and the grating angle, because some special scan modes are often used, for instance, to suppress the higher spectroscopic orders.

In the present paper, we propose a novel design concept using the complete light-path function for a variable-included-angle Monk–Gillieson monochromator with VLS gratings, and demonstrate several advantages of the monochromator. This paper is organized in the following manner: §2 describes the design principle of the monochromator; in §3 we present a design example for an undulator beamline and estimate the energy resolution; the results are compared with a similar beamline with diverging illumination on the VLS gratings in §4; in §5 we apply the new design concept to a higher-resolution monochromator with the same undulator source, as well as a medium resolution one with a rather high-emittance bending-magnet source; and concluding remarks are briefly given in §6.

2. Design principle

The layout of the Monk–Gillieson mounting monochromator with a VLS grating is schematically illustrated in Fig. 1. Although either sagittal (*a*) or meridional (*b*) focusing is available to realise converging illumination on the grating, sagittal focusing might be suitable for recent low-emittance X-ray sources, because the effect of the slope error is reduced compared with meridional focusing. In contrast, sagittal focusing is not suitable for high-divergence sources such as a bending magnet, because it may cause serious aberrations. In such a case, meridional focusing with a toroidal mirror may still cause significant aberrations. Therefore, we assume the use of toroidal and cylindrical (or spherical) mirrors for the sagittal and meridional focusing configurations, respectively. Although an additional mirror for horizontal focusing is necessary in the case of meridional focusing (*b*), it does not affect the resolution of the monochromator.

X-rays generated at A are vertically converged by a focusing mirror, FM, the incidence angle of which is η_A. The distance between the virtual focal point B′ and a VLS grating, G, is $-r_A$, where r_A is

 DOI: 10.1107/S0909049503023598

defined as a negative value because B′ is located behind G. The included angle at G is varied by an off-axis rotation of a plane mirror, PM (Petersen, 1982). Here, the included angle is defined as $2K = \alpha - \beta$, where α and β are the incidence and diffraction angles of G, which have positive and negative values, respectively. The diffracted X-rays are monochromated by narrowing an exit slit, whose centre is located at B. The A–FM, FM–PM, PM–G and G–B distances are denoted by p_A, q_{A1}, q_{A2} and r_B, respectively, as indicated in Fig. 1.

The groove parameters for the VLS grating are given by expanding the groove number, n, from the centre of the grating in a power series in the position on the grating, w,

$$n = n_{10}w + (n_{20}w^2)/2 + (n_{30}w^3)/2 + (n_{40}w^4)/8 + \ldots, \qquad (1)$$

where w is defined along the light-propagation direction and n_{i0} are expansion coefficients. For X-rays passing through B after being reflected by FM and PM and diffracted by G, the light path function, F, is defined by

$$\begin{aligned} F = {} & p_A + q_A + r_B \\ & + M_{10}w + (M_{20}w^2 + M_{02}l^2 + M_{30}w^3 + M_{12}wl^2)/2 \\ & + (M_{40}w^4 + M_{22}w^2l^2 + M_{04}l^4)/8 + \ldots \\ & + [n_{10}w + (n_{20}w^2)/2 + (n_{30}w^3)/2 + (n_{40}w^4)/8 + \ldots]m\lambda, \end{aligned} \qquad (2)$$

where $q_A = q_{A1} + q_{A2}$, m is the diffraction order (1 in the present case) and λ is the wavelength of the X-rays. Although q_A changes slightly as a function of photon energy, the effect of this small change is negligible, so we can assume that q_A is constant. The coefficients M_{ij}, including the effects of FM, are deduced in a manner similar to that of Namioka & Koike (1995), some of which are given by

$$\begin{aligned} M_{10} &= -\sin\alpha - \sin\beta, \\ M_{20} &= (\cos^2\alpha)/r_A + (\cos^2\beta)/r_B, \\ M_{30} &= (\sin\alpha\cos^2\alpha)/r_A^2 + (\sin\beta\cos^2\beta)/r_B^2 \\ &\quad \text{(sagittal focusing) or} \\ M_{30} &= (\sin\alpha\cos^2\alpha)/r_A^2 + (\sin\beta\cos^2\beta)/r_B^2 - [2(A_{10})_A^2K_A]/R_A \\ &\quad \text{(meridional focusing),} \end{aligned} \qquad (3)$$

where

$$\begin{aligned} r_A &= q_A + [1/p_A - (2\cos\eta_A)/\rho_A]^{-1} \text{ (sagittal focusing) or} \\ r_A &= q_A + [1/p_A - (2\sec\eta_A)/R_A]^{-1} \text{ (meridional focusing),} \\ (A_{10})_A &= -(\cos\alpha)/(A_A q_A \cos\eta_A), \\ A_A &= 1/p_A + 1/q_A - (2\sec\eta_A)/R_A, \\ K_A &= (\cos\alpha)/r_A - (A_{10})_A/R_A. \end{aligned} \qquad (4)$$

Here, R_A and ρ_A are the meridional and sagittal radii of FM, respectively. Note that some expressions for sagittal focusing are different from those for meridional focusing (Amemiya *et al.*, 1996).

First, we optimize the parameters concerning the focusing condition by selecting two optimization energies, E_1 (included angle, $2K = 2K_1$) and E_2 ($2K = 2K_2$). It should be emphasized that one can freely choose n_{10} (corresponding to the groove density at the centre of the grating), E_1, E_2, K_1 and K_2 according to the experimental requirements, such as the energy range, energy resolution and photon flux. r_A (corresponding to R_A and ρ_A for meridional and sagittal focusing, respectively) and n_{20} are determined so that

$$\begin{aligned} M_{20} + n_{20}m\lambda_1 &= 0 \qquad (2K = 2K_1), \\ M_{20} + n_{20}m\lambda_2 &= 0 \qquad (2K = 2K_2), \end{aligned} \qquad (5)$$

where λ_1 and λ_2 are the wavelengths corresponding to E_1 and E_2, respectively. As for the other photon energies, the included angle, $2K$, is determined by solving the following equation at each energy with the aid of equation (3),

$$M_{20} + n_{20}m\lambda = 0. \qquad (6)$$

Accordingly, the defocus aberration vanishes over the whole energy range by properly changing the included angles. Then n_{30} and n_{40} are similarly optimized by solving the following equations at E_3 and E_4,

$$\begin{aligned} M_{30} + n_{30}m\lambda_3 &= 0, \\ M_{40} + n_{40}m\lambda_4 &= 0, \end{aligned} \qquad (7)$$

where λ_3 and λ_4 are again the wavelengths corresponding to E_3 and E_4, respectively.

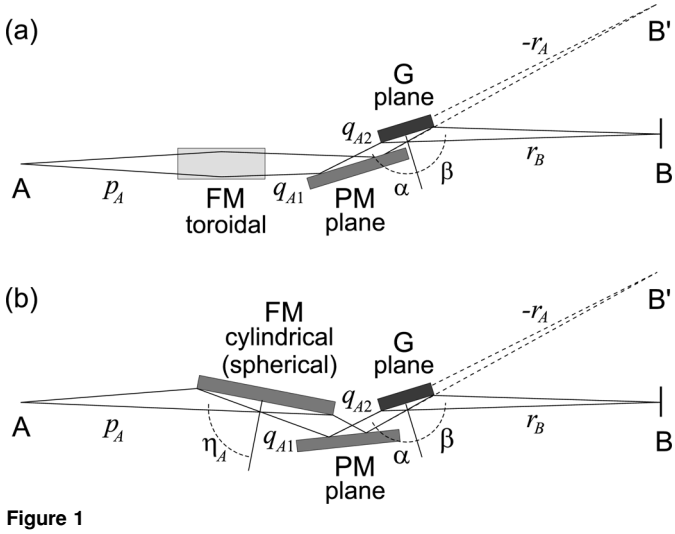

Figure 1
Schematic diagram of a variable-included-angle Monk–Gillieson mounting monochromator with a varied-line-spacing (VLS) plane grating in (*a*) sagittal and (*b*) meridional focusing configurations.

3. Design example for an undulator beamline

In order to demonstrate the validity of the new design concept described in the previous section, we designed a beamline with a typical undulator source and estimated the energy resolution of the beamline using the ray-tracing program *XRAY-T* (Amemiya *et al.*, 2002). A layout of the designed beamline is depicted schematically in Fig. 2(*a*), together with the optical parameters for the mirrors and gratings. The beamline components are the same as those illustrated in Fig. 1(*a*), except for a refocusing mirror, M3, which does not affect the performance of the monochromator. We chose the following optimization parameters for a 600 lines mm^{-1} grating; E_1 = 50 eV, K_1 = 164°, E_2 = 500 eV, K_2 = 174° and $E_3 = E_4$ = 100 eV. The included angle at E_3 (= E_4) was 167.60°, which was obtained by solving equation (6). For convenience, let us express the groove parameters of the VLS grating in another form by expanding the groove density, N, with coefficients a_i,

$$N = \mathrm{d}n/\mathrm{d}w = N_0(1 + a_1w + a_2w^2 + a_3w^3 + \ldots), \qquad (8)$$

where N_0 is the groove density at the centre of the grating. Then the optimized parameters for the grating with N_0 (= n_{10}) = 600 mm^{-1} are $a_1 = -1.2630 \times 10^{-4}$ mm^{-1}, $a_2 = 1.2 \times 10^{-8}$ mm^{-2} and $a_3 = -1.7 \times 10^{-12}$ mm^{-3}, corresponding to $n_{20} = -7.5780 \times 10^{-2}$ mm^{-2}, $n_{30} = 4.7 \times 10^{-6}$ mm^{-3} and $n_{40} = -2.0 \times 10^{-9}$ mm^{-4}, respectively. The sagittal radius of M1 was determined to be ρ_A = 0.643 m, corresponding to $r_A = -14.899$ m. The groove parameters for a

1200 lines mm^{-1} grating were obtained by simply making N_0 = 1200 mm^{-1}, without changing a_1, a_2 or a_3.

For the ray-tracing simulation, a 4.5 m-long undulator source with the following electron-beam parameters was assumed: σ_x = 350 µm, σ_y = 20 µm, σ_x' = 20 µrad and σ_y' = 5 µrad. A typical example of the ray-traced beam profile is shown in Fig. 3, from which the energy resolution was estimated to be ∼1/26000. Here, the energy resolution is defined as $\Delta\lambda/\lambda$, where $\Delta\lambda = 2.688 s_\lambda$, and s_λ is the product of the standard deviation of ray-traced spots in the direction of dispersion and the reciprocal linear dispersion at λ (Koike & Namioka, 1995). Note here that the estimated energy resolution does not include the slope-error effect, which may cause a deterioration of the resolution. In fact, the slope-error limited resolution was estimated to be ∼1/24000 at 100 eV, assuming a 0.1 arcsec slope error on both the VLSG and M2. The estimated energy resolution is plotted in Fig. 4 as a function of photon energy, together with the source-size and slope-error limited resolutions. Again, a 0.1 arcsec slope error on both the VLSG and M2 was assumed. Although the practical resolution seems to be limited by the slope error, it should be emphasized that a slope error of 0.1 arcsec or even less is technically available at the present time. If the slope error is small enough, the resolution is limited by the source size over the whole energy range, as indicated in Fig. 4.

One of the greatest advantages of the new design concept is clarified in Fig. 5, where the photon energy is scanned by rotating only the VLS grating with a fixed included angle. Although this results in a finite defocus aberration, the high resolution is kept over a rather wide energy range. Therefore, the photon energy can be scanned by rotating the grating only, which gives a stable energy scale. The energy resolution limited by the defocus aberration is also plotted in Fig. 5, implying that the defocus aberration does not affect the resolution so severely. This is because the focal plane of the Monk–Gillieson mounting VLS grating monochromator is almost perpendicular to the beam direction at the exit slit. In order to clarify this advantage, a contour plot for the energy resolution as a function of photon energy and included angle is depicted in Fig. 6. Here, the energy resolution was estimated as a convolution of the source-size and aberration limited resolutions, as indicated in Fig. 7 for the 600 lines mm^{-1} grating. One can obtain moderate resolution in

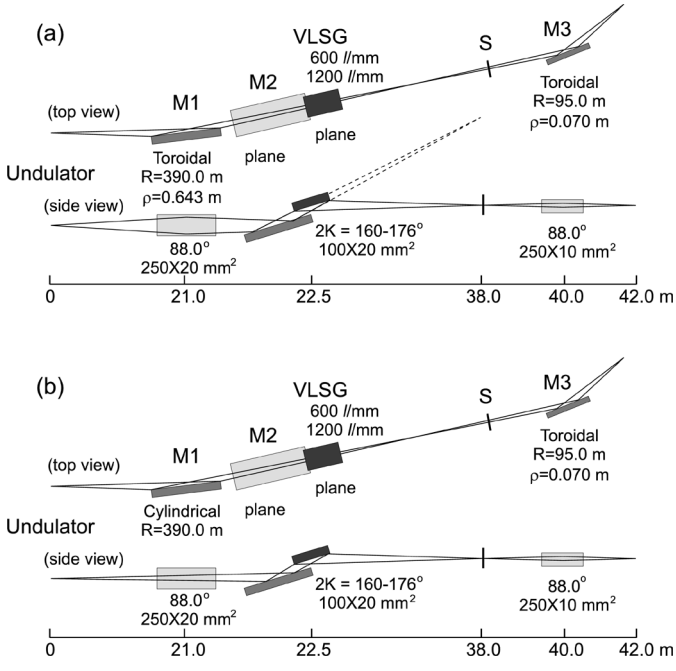

Figure 2
Schematic layout of an undulator-based beamline with (*a*) converging and (*b*) diverging illumination on the VLS gratings.

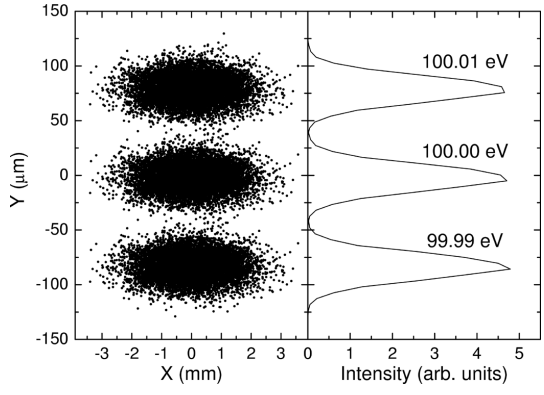

Figure 3
Beam profile at the exit slit simulated by the ray-tracing program *XRAY-T* (Amemiya *et al.*, 2002). The resolving power was estimated as $\Delta\lambda/\lambda$ ∼1/26000 at 100 eV from the splitting of three different energies (100 ± 0.01 eV) at the exit slit (Koike & Namioka, 1995).

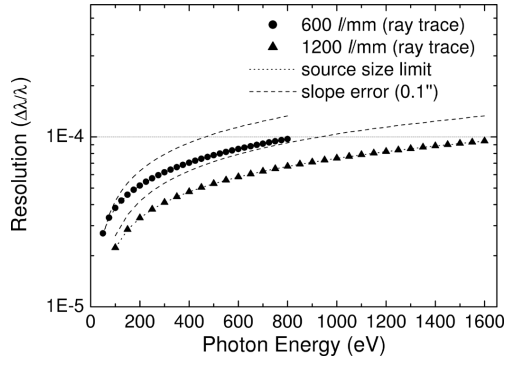

Figure 4
Energy resolution, $\Delta\lambda/\lambda$, for 600 (circles) and 1200 lines mm^{-1} (triangles) gratings with the ideal included angle estimated from the ray-traced spots, together with the source-size (dotted lines) and slope-error (dashed lines) limited resolutions.

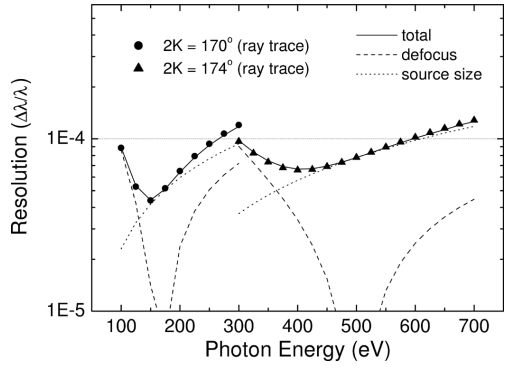

Figure 5
Energy resolution, $\Delta\lambda/\lambda$, for a 600 lines mm^{-1} grating with included angles fixed at 170 (circles) and 174° (triangles) estimated from the ray-traced spots, together with the defocus (dashed lines) and source-size (dotted lines) limited resolutions. The total of the source-size and aberration (defocus, coma and spherical) limited resolutions is also plotted (solid lines).

almost all possible conditions, while high resolution can be achieved over a rather wide region around the ideal included angle.

4. Comparison with diverging illumination on the VLS grating

Although one may think that the above-mentioned advantage is due to the small divergence of the undulator source, the situation is completely different in the case of diverging illumination on the grating, even if one adopts the same undulator. We designed a beamline, shown in Fig. 2(*b*), which has a cylindrical first mirror, M1, instead of a toroidal one. Therefore, X-rays are only converged in the horizontal direction, resulting in diverging illumination on the VLS gratings, VLSG. We optimized the groove parameter, a_1, of a 600 lines mm^{-1} grating so that the defocus aberration vanishes at 500 eV with the included angle, $2K$, of 174°, yielding $a_1 = -2.3535 \times 10^{-4}$ mm^{-1}. The defocus aberration for the other photon energies can be eliminated by properly changing $2K$. Then a_2 and a_3 were optimized at 100 eV ($2K = 166.54°$), resulting in $a_2 = 1.5 \times 10^{-8}$ mm^{-2} and $a_3 = -1.7 \times 10^{-12}$ mm^{-3}. Again, the groove parameter for a 1200 lines mm^{-1} grating was obtained by simply making $N_0 = 1200$ mm^{-1}, without changing a_1, a_2 or a_3.

Fig. 8 gives energy resolutions with the ideal and fixed included angles, estimated by the ray-tracing program. All the parameters for the undulator source are the same as those in the previous section. In spite of the fact that vertical focusing must only be provided by the grating, a resolution comparable with that of the beamline with converging illumination on the grating (Fig. 4) can be achieved by properly changing the included angles. However, a slight change in the photon energy with a fixed included angle causes a serious lowering of the resolution, as indicated in Fig. 8(*b*). It is thus impossible to scan the photon energy with only the rotation of the grating while maintaining high resolution. Fig. 9 depicts a contour plot for the energy resolution as a function of photon energy and included angle, indicating that even medium resolution, such as 1/1000, can only be achieved in a small area around the ideal included angle. This is an inevitable disadvantage of these optics, in which focusing must be achieved by the grating only.

5. Design variations

The design procedure described in §3 is quite flexible, since one can freely choose the optimization energies, E_1–E_4, and included angles, K_1 and K_2. For instance, a higher energy resolution can be achieved by reducing the source-size effect on the resolution by increasing the

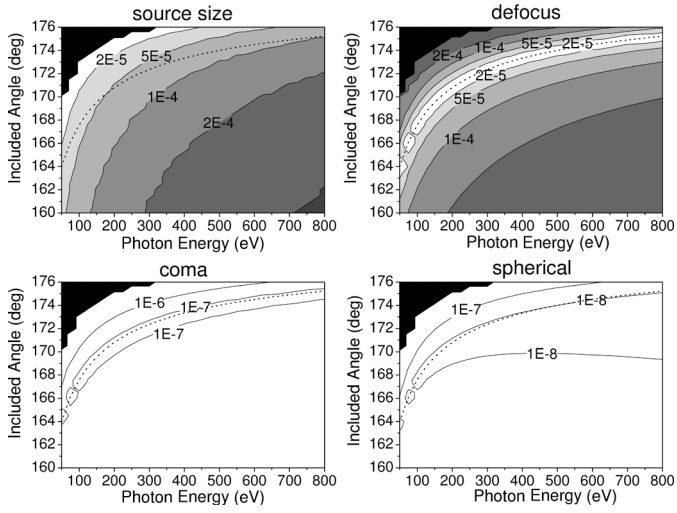

Figure 7
Contour plot for the source-size and aberration limited energy resolution as a function of photon energy and included angle for a 600 lines mm^{-1} grating.

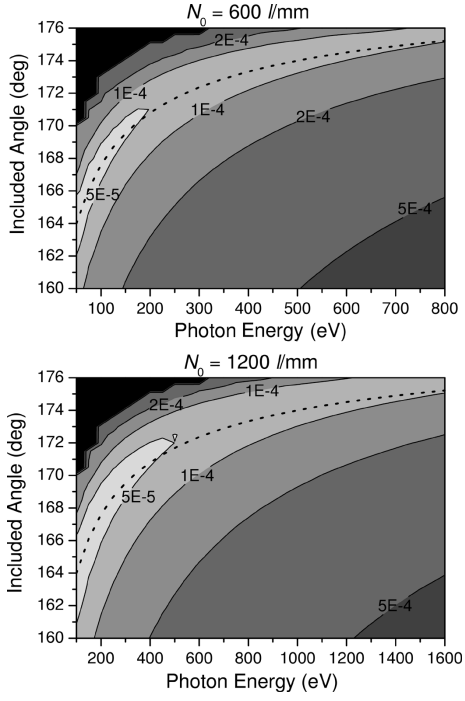

Figure 6
Contour plot for the total of the source-size and aberration (defocus, coma and spherical) limited resolutions as a function of photon energy and included angle for 600 (top) and 1200 lines mm^{-1} (bottom) gratings. The defocus aberration vanishes on the dotted line, which represents the ideal included angle.

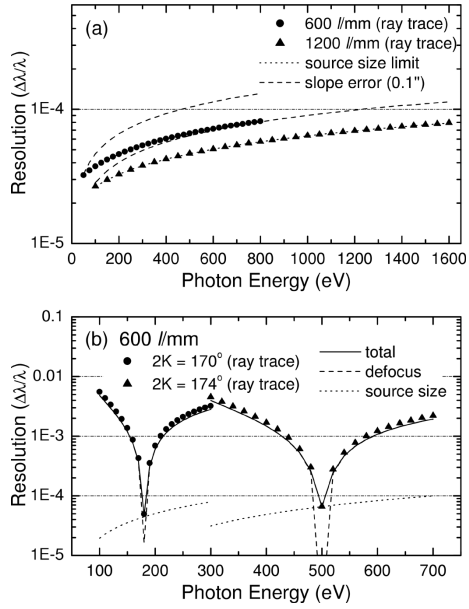

Figure 8
Energy resolution, $\Delta\lambda/\lambda$, for a beamline with diverging illumination on VLS gratings with (*a*) ideal and (*b*) fixed included angles estimated from the ray-traced spots, together with the source-size (dotted lines), slope-error [dashed lines in (*a*)] and defocus [dashed lines in (*b*)] limited resolutions. The total of the source-size and aberration (defocus, coma and spherical) limited resolutions (solid lines) is also plotted in (*b*).

$\cos\beta/\cos\alpha$ ratio, sacrificing photon intensity. We designed a beamline in order to obtain a higher resolution than that for the beamline depicted in Fig. 2(*a*), without changing the undulator source and beamline layout. We used the following optimization parameters for a 600 lines mm^{-1} grating: E_1 = 50 eV, K_1 = 168°, E_2 = 500 eV, K_2 = 175° and $E_3 = E_4$ = 100 eV. Again, the groove parameter for a 1200 lines mm^{-1} grating was obtained by simply making N_0 = 1200 mm^{-1}. The optimized parameters are $a_1 = -1.2783 \times 10^{-4}$ mm^{-1}, $a_2 = 1.2 \times 10^{-8}$ mm^{-2}, $a_3 = -1.1 \times 10^{-12}$ mm^{-3} and ρ_A = 0.645 m ($r_A = -14.982$ m). The estimated energy resolution is plotted in Fig. 10. A higher energy resolution is obtained compared with that shown in Figs. 4 and 5, owing to the reduced source-size effect. Note here that the slope-error effect is also reduced.

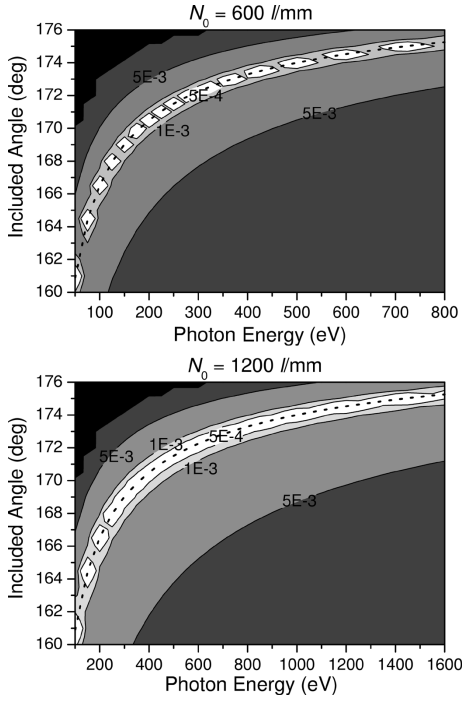

Figure 9
Contour plot for the total of the source-size and aberration (defocus, coma and spherical) limited resolution as a function of photon energy and included angle for a beamline with diverging illumination on VLS gratings. The defocus aberration vanishes on the dotted line, which represents the ideal included angle.

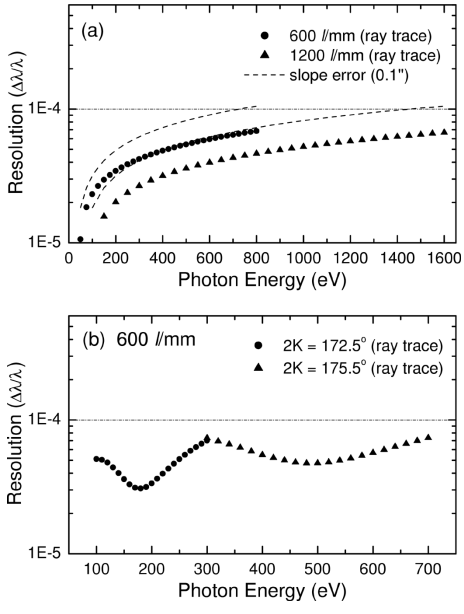

Figure 10
Energy resolution, $\Delta\lambda/\lambda$, for a higher-resolution beamline with converging illumination on the VLS gratings with (*a*) ideal and (*b*) fixed included angles estimated from the ray-traced spots. The slope-error limited resolution (dashed lines) is also plotted in (*a*).

Next, we designed a beamline with a bending-magnet source, as illustrated in Fig. 11, in order to confirm that the present design concept is also valid for rather high-emittance X-ray sources. The electron-beam parameters were assumed as follows, and are similar to those for the Photon Factory: σ_x = 350 µm, σ_y = 75 µm, $\sigma_{x'}$ = 200 µrad and $\sigma_{y'}$ = 20 µrad. Since the electron-beam size is rather large, we inserted an entrance slit, S1, which is regarded as the source point, A, in Fig. 1. X-rays from the bending magnet are horizontally converged by M1 and vertically focused on S1 by M2. The other optical components are similar to those shown in Fig. 2(*a*), except for a meridional focusing mirror, M3. We adopted the same optimization

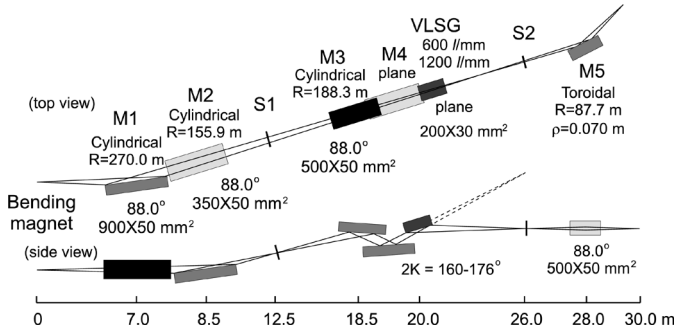

Figure 11
Schematic layout of a bending-magnet beamline with converging illumination on VLS gratings.

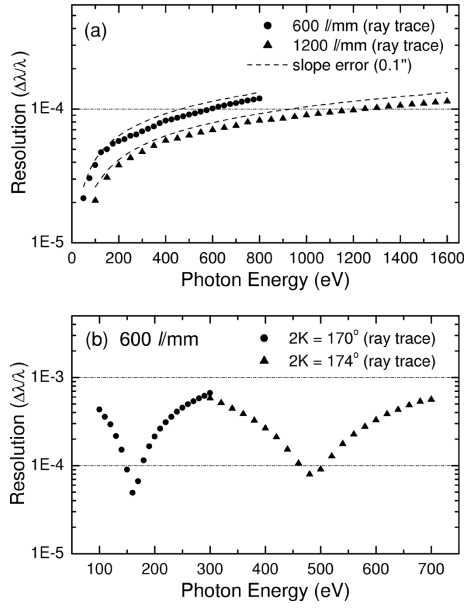

Figure 12
Energy resolution, $\Delta\lambda/\lambda$, for a bending-magnet beamline with converging illumination on VLS gratings with (*a*) ideal and (*b*) fixed included angles estimated from the ray-traced spots. The entrance slit opening was assumed to be 20 µm. The slope-error limited resolution (dashed lines) is also plotted in (*a*).

energies and included angles for a 600 lines mm^{-1} grating as those for the beamline described in §3: E_1 = 50 eV, K_1 = 164°, E_2 = 500 eV, K_2 = 174° and $E_3 = E_4$ = 100 eV. The optimized parameters are $a_1 = -3.2627 \times 10^{-4}\,mm^{-1}$, $a_2 = 9.4 \times 10^{-8}\,mm^{-2}$, $a_3 = -4.2 \times 10^{-12}\,mm^{-3}$ and R_A = 188.4 m (r_A = −5.767 m). The estimated resolution with an entrance-slit opening of 20 μm is given in Fig. 12. It can be seen that rather high resolution is achieved, though ∼80% of the original X-rays are lost at the entrance slit, which is inevitable in the case of a high-emittance bending-magnet source. The advantage of the new design concept is still maintained, as shown in Fig. 12(*b*): medium resolution is achieved over a wide energy range. It should be emphasized that the energy resolution is better than that for the beamline with diverging illumination (Fig. 10) if one scans only the grating, in spite of the significant difference in the X-ray sources.

6. Conclusions

We have proposed a novel design concept for a variable-included-angle Monk–Gillieson mounting monochromator with a varied-line-spacing (VLS) plane grating, in which the grating is illuminated by converging X-rays. The validity of the new concept has been demonstrated using the ray-tracing method for a beamline with a typical undulator source. A design example for a bending-magnet beamline has also been presented, indicating that the new concept is valid even for high-emittance sources. The advantages of the proposed design concept are summarized as follows:

(*a*) One can freely choose two energies and two included angles for optimization concerning the defocus aberration, which allows a flexible beamline design according to the experimental requirements.

(*b*) High energy resolution is achieved over a wide energy range by properly changing the included angle.

(*c*) Relatively high resolution is maintained even if one scans the photon energy with a fixed included angle, which is a great advantage over monochromators with diverging illumination on the VLS grating (Itou *et al.*, 1989). This allows various scan modes, such as a higher-order suppression mode, while maintaining rather high resolution.

(*d*) No focusing mirror is necessary downstream of the grating. This makes the beamline optics simple and reduces the slope-error effect of the mirror.

The authors gratefully acknowledge Professor Akira Yagishita (Photon Factory), Dr Masato Koike (Japan Atomic Energy Research Institute) and Professor Shoji Suzuki (Tohoku University) for their invaluable comments and discussion concerning the monochromator design.

References

Amemiya, K., Kitajima, Y., Ohta, T. & Ito, K. (1996). *J. Synchrotron Rad.* **3**, 282–286.
Amemiya, K., Kondoh, H., Yokoyama, T. & Ohta, T. (2002). *J. Electron Spectrosc. Relat. Phenom.* **124**, 151–164.
Follath, R. & Senf, F. (1997). *Nucl. Instrum. Methods A*, **390**, 388–394.
Gillieson, A. H. C. P. (1949). *J. Sci. Instrum.* **26**, 335–339.
Hettrick, M. C. (1988). *Nucl. Instrum. Methods A*, **266**, 404–413.
Hettrick, M. C., Underwood, J. H., Batson, P. J. & Eckart, M. J. (1988). *Appl. Opt.* **27**, 200–202.
Itou, M., Harada, T. & Kita, T. (1989). *Appl. Opt.* **28**, 146.
Koike, M. (1996). US Patent 5 528 364.
Koike, M. & Namioka, T. (1995). *Rev. Sci. Instrum.* **66**, 2144–2146.
Monk, G. S. (1928). *J. Opt. Soc. Am.* **17**, 258–368.
Namioka, T. & Koike, M. (1995). *Appl. Opt.* **34**, 2180–2186.
Petersen, H. (1982). *Opt. Commun.* **40**, 402–206.